Original Research Article

Automatic frontal sinus recognition in computed tomography images for person identification

Luis A. de Souza Jr.[a,*], Aparecido N. Marana[a], Silke A.T. Weber[b]

[a] *São Paulo State University (UNESP), Department of Computing, Faculty of Sciences, Bauru, SP, Brazil*
[b] *São Paulo State University (UNESP), Department of Ophthalmology and Otorhinolaryngology, Botucatu Medical School, Botucatu, SP, Brazil*

A B S T R A C T

In many cases of person identification the use of biometric features obtained from the hard tissues of the human body, such as teeth and bones, may be the only option. This paper presents a new method of person identification based on frontal sinus features, extracted from computed tomography (CT) images of the skull. In this method, the frontal sinus is automatically segmented in the CT image using an algorithm developed in this work. Next, shape features are extracted from both hemispheres of the segmented frontal sinus by using BAS (Beam Angle Statistics) method. Finally, L_2 distance is used in order to recognize the frontal sinus and identify the person. The novel frontal sinus recognition method obtained 77.25% of identification accuracy when applied on a dataset composed of 310 CT images obtained from 31 people, and the automatic frontal sinus segmentation in CT images obtained a mean Cohen Kappa coefficient equal to 0.8852 when compared to the ground truth (manual segmentation).

© 2018 Elsevier B.V. All rights reserved.

1. Introduction

Biometric identification refers to the use of physical or behavioral characteristic to determine the person identity. In order to be used for person biometric identification a physical or behavioral characteristic must have some properties such as: universality, uniqueness, permanence, and acceptability [1].

Fingerprints and faces characteristics are frequently used for person biometric identification in commercial, banking, and government applications [1]. However, for the identification of deceased people, in forensic applications, these characteristics are not always available, because they derive from soft tissues of the human body that decomposes soon after death. In these cases, DNA features could be an alternative. However, in carbonized bodies, for instance, the characteristics of DNA cannot always be recovered [2]. Besides, DNA analysis is very expensive for applying to every case and it is not reliable in some cases as dry bones [3]. Therefore, in many human identification situations, the use of biometric features extracted from the bones, the hardest tissues of the human body, such as the frontal sinus features, may be the only option.

Frontal sinus consists of a paired irregularly shaped loculated cavity, located in the frontal bone [4]. The uniqueness property of the frontal sinus was first observed by Zuckerkandl, in 1875, when

he called attention to its asymmetric morphology [5]. In 1927, Culbert and Law described the first human identification through morphological analysis of frontal sinus that was accepted in a United States court of law [6]. In 1943, Schuller was the first to suggest the possibility of identifying a deceased person by comparing frontal sinus radiography images [7]. In the beginning of 21st century, Ribeiro [8] and Kirk, Wood and Goldstein [9] reported positive results in skeletal identification using frontal sinus information extracted from radiography (X-ray) images.

The frontal sinus asymmetry, among other particular characteristics, has motivated several studies in the last few decades aiming people identification through the analysis of frontal sinus measurements obtained from X-ray films. Many of these studies have established that the highly variable radiographic pattern of the frontal sinus is unique to every individual, even among monozygotic twins [7–10].

The frontal sinus is increasingly being used for postmortem human identification. In 2007, Tatlisumak et al. [3] defined a system for the identification of unknown bodies by using computed tomography images of frontal sinus. This system, called FSS, included simple features as F (presence or absence of frontal sinus), S (intersinus and intrasinus septum) and S (scalloping). Measurements selected for this study were width, height, anteroposterior length, total width of two sinuses, the distance between the highest points of the two sinuses and the distance of each sinus to its maximum lateral limit. All the features and measurements were coded according to the FSS system defined for

---

* Corresponding author.
E-mail address: luis.souza@fc.unesp.br (L.A. d. Souza).

each case and coded formulas were compared. At least 93% of the formulas could be eliminated for a case by using FSS system.

In 2015, Soares et al. [11] performed a study to evaluate the applicability of human identification parameters, established by Tatlisumak et al. [3], using cone-beam computed tomography tridimensional reconstruction and extraoral radiographs of the frontal sinus. They concluded that, despite some advantages of using X-ray, such as the low costs, comparison of radiographic images has limitations because it is a subjective test that depends on the expert's experience and the radiographic image can vary significantly according to the incidence of the X-ray beam. They recommend the use of CT imaging examination for proper study of the paranasal sinuses, since it enables the acquisition of sectional images, three-dimensional scans of the sinuses, and eliminates the structural overlapping observed in X-ray images.

In 2015, Hashim et al. [12] made a study that tested the practical relevance of prescribing superimposition by superimposing ante-and-post-mortem frontal sinus patterns recorded in real case situations and ante-and-post-mortem of frontal sinus patterns in simulated cases, recorded using archived skulls, resulting in a perfect match of radiographs from the same skull only when the orientation of the skull obtained for the first (simulated ante-mortem) recording is unaltered for the second (simulated post-mortem) recording. According to the authors, for the real life cases, normally the superimposition is not possible.

In 2016, Rabelo et al. [13] studied the applicability of the FSS system proposed by [3] in order to identify persons, by means of the frontal sinus measures acquired from frontal and lateral cephalometric radiographs. They reported good results.

Researches also have been carried out in order to identify gender by analyzing measurements of the frontal sinuses obtained from X-ray films. Belaldavar et al. [14], for instance, concluded that the area, height and width of the frontal sinuses are, in average, bigger in men than in women. Uthman et al. [15] and Carvalho et al. [16], conducted experiments focusing gender discrimination and human identification using CT images and structures of the paranasal sinuses (frontal sinuses and other cranial structures).

In general, these previous works are based on manual or semi-automatic frontal sinus segmentation methods. The review by Xavier, Terada and Silva [17] showed that there were no fully automatic frontal sinus segmentation method proposed in literature so far.

Another characteristic of previous works is that they are based on X-ray images. However, computed tomography (CT) images allow better frontal sinuses segmentation and recognition than X-ray images because of the better contrast provided by the CT technology. Fig. 1 shows an X-ray image and a computed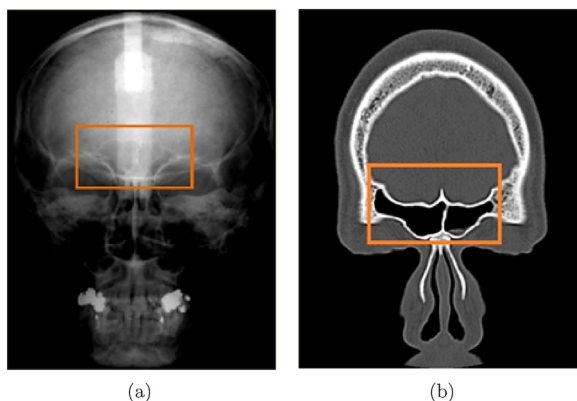 tomography (CT) image of two distinct individuals, with the frontal sinuses enclosed by rectangles. One can observe that the CT image (right) allows an easier and better analysis of the frontal sinus structures, when compared to the X-ray image (left). Besides, CT scans produce sequences of images, allowing 3D analysis of the frontal sinus structures.

The goal of our work is to propose and develop a fully automatic and robust method for frontal sinus segmentation and recognition using computed tomography images to be used for person identification.

2. Frontal sinus

Frontal sinus consists of a paired irregularly shaped loculated cavity, located in the frontal bone, which communicate with the nasal fossa via the infundibulum [4]. This cavity develops embryonically from an ethmoidal cell and is not visible at birth. It starts developing during the second year of life, reaching its maximum size at the age of 20.

As the frontal sinus remains stable even after death [4,10] it is very suitable for post mortem person identification. The configuration of the frontal sinus is claimed to be unique for each individual [4,7,9,10] and is controlled by genetic and environmental factors. Frontal sinus variations have been reported in the literature even for monozygotic twins [4,10].

Fig. 2 shows three CT images of three different individuals. As one can observe in the red rectangles, the three frontal sinuses have very distinct and particular characteristics that can be used to identify the individuals.

3. Proposed method

The new method proposed in this work for person identification based on frontal sinus features extracted from computed tomography images has three main stages:

- Frontal sinus segmentation;
- Frontal sinus feature extraction; and
- Frontal sinus recognition.

3.1. Frontal sinus segmentation

The frontal sinus segmentation stage consists in automatically detecting in CT images the pixels belonging to the internal region of the frontal sinus.

The first step of this process is the binarization of the gray level CT image, which is carried out by replacing the original gray scale pixel values by 0 or 1, according to a threshold value. This technique was chosen because it is fast and results in very good quality segmentation since CT images present high contrast in the frontal sinus region, as one can observe in Fig. 2 (black regions completely surrounded by white borders).

In our method, the threshold value used for binarization is automatically defined. Given I, an $m \times n$ CT image, its gray level histogram H is calculated. Then, by considering the rightmost mode (m_r) of H, cranial bones regions in the CT images can be easily detected since they are associated with the brighter regions of I. So, the threshold value (t) of the binarization stage is taken as 80% of m_r.

Fig. 3(b) shows the logarithm of the gray level histogram H of the CT image of Fig. 3(a), with the threshold t represented by the vertical red line located at the left side of the rightmost mode of H. Fig. 3(c) shows the binary image B_1 obtained automatically with the binarization process applied to the gray level CT images I presented in Fig. 3(a).

After this first binarization, the next step is to find the region of interest (ROI) of the CT image, that is, the smaller rectangle that contains the frontal sinus. An initial ROI, called R_1, is taken as the

Fig. 1. Frontal sinuses enclosed by rectangles: (a) X-ray image and (b) computed tomography image.
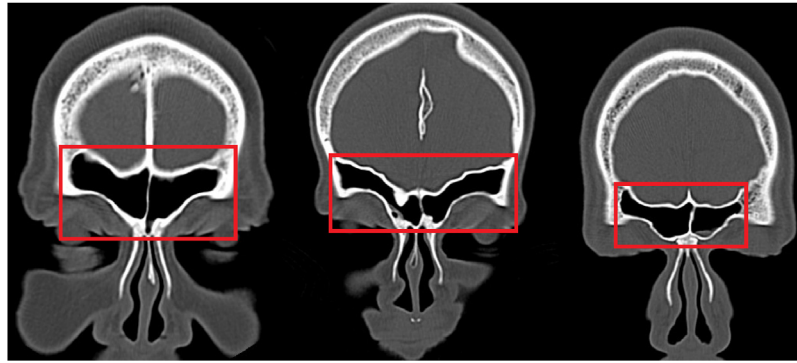
Fig. 2. CT images of different individuals. The frontal sinuses are highlighted by red rectangles. (For interpretation of the references to color in this figure legend, the reader is referred to the web version of this article.)

rectangle defined by the top and bottom straight lines found in the binary image B_1 by using the function g, defined in Eq. (1), and by the left and right straight lines found in the binary image B_1 by using the function f, defined in Eq. (2),

$$g(i) = \sum_{j=1}^{n} B_1(i,j), \quad i = 1, \ldots, m. \tag{1}$$

$$f(j) = \sum_{i=1}^{m} B_1(i,j), \quad j = 1, \ldots, n. \tag{2}$$

with m and n being the height and the width of B_1, respectively.

Fig. 4 shows the four straight lines that define the top, bottom, left, and right limits of R_1, found in the binary image B_1, by using the Eqs. (1) and (2).

The left and right straight lines correspond, respectively, to the leftmost and the rightmost columns of B_1 for what the function f is different of zero, while the top and the bottom straight lines correspond, respectively, to the topmost and the bottommost rows of B_1 for what the function g is different of zero.

One can observe in Fig. 4 that the ROI R_1 encloses the cranial region of the CT image. However, our goal is to find the smaller rectangle that encloses the frontal sinus. Then, a new ROI, called R_2, is calculated from R_1. A new image I_2 is calculated by cropping the image I, using the R_1 limits. From I_2, a new binary image, called B_2, is calculated considering as threshold the leftmost mode of the gray level histogram H plus 1. The binarization applied is described by Eq. (3).

$$B_2(i,j) = \begin{cases} 0, & \text{if } I_2(i,j) \geq \text{threshold} \\ 1, & \text{otherwise} \end{cases} \tag{3}$$

In this second binarization process, all pixels with gray levels values equal or above the threshold are set to 0 (black), while all pixels with gray level values below to the threshold are set to 1 (white).

Fig. 5(a) shows the image I_2 obtained by cropping the image I, presented in Fig. 3(a), using the ROI R_1 limits. Fig. 5(b) shows the new binary image B_2 obtained after the second binarization process.

In order to find the bottom and top limits of the white structure inside B_2, the function g (Eq. (1)) is applied to B_2.

It is possible to observe in Fig. 6 that at the beginning, as i increases from 0 to m, the values of $g(i)$ decreases, due the round shape of the skull that forms a white region in the left and right top corners of the binary image B_2, or keep constant until i reaches the value of the first row (top row) that intersects the frontal sinus region. After that, the values of $g(i)$ start increasing, as the value of i increases. So, we are able to identify the top limit of the R_2 region by identifying the leftmost value of i, that we called x_1, for what $g(i)$

starts growing. On the other side, as i decreases from m to 0, the values of $g(i)$ decreases, due the round shape of the skull that forms a white region in the left and right bottom corners of the binary image B_2, or keep constant until i reaches the value of the first row (bottom row) that intersects the frontal sinus (or other nearby cavity) region. After that, the values of $g(i)$ start increasing, as the value of i decreases. So, we are able to identify the bottom limit of the R_2 region by identifying the rightmost value of i, that we called x_2, for what $g(i)$ starts growing.

Fig. 7 shows the binary image, B_3, obtained by cropping B_2, using the R_2 limits. One can observe in Fig. 7 that B_3 is composed by a number of white regions corresponding to the frontal sinus and other structures. Because some of these regions do not belong to the frontal sinus, a new region of interest, called R_3, is found containing only the white regions of the frontal sinus. The algorithm used for this purpose is presented in Algorithm 1.

**Algorithm 1.** Algorithm to calculate the ROI R_3.

---

1 **Input:** Binary image B_3, ROI R_2 ;
2 **Output:** ROI R_3;
3 $R_3 \leftarrow R_2$;
4 $g \leftarrow$ function g applied to B_3;
5 **for** $j \leftarrow 1$ to high of B_3 **do**
6   **if** $g(j) = 0$ **then**
7   bottom limit of $R_3 \leftarrow j$;
8   exit();
9   **end**
10 **end**
11 $h_{R_2} \leftarrow (high$ of $R_2)/2$;
12 $Img \leftarrow \emptyset$;
13 $S \leftarrow$ list of white connected regions of B_3;
14 $i \leftarrow 1$;
15 **while** $S \neq \emptyset$ **do**
16     $c \leftarrow$ centroid of S_i;
17   **if** $(c_x < h_{R_2})$ AND $(S_i$ does not surpass $h_{R_2})$ **then**
18         $Img \leftarrow Img \cup S_i$;
19         $S \leftarrow S - S_i$;
20   **end**
21     $i \leftarrow i + 1$;
22 **end**
23 top limit of $R_3 \leftarrow$ top limit of Img;
24 bottom limit of $R_3 \leftarrow$ bottom limit of Img;

As one can observe in Algorithm 1 there are two ways to define the ROI R_3. Initially R_3 is taken as R_2 (line 3). Then, the function g (Eq. (1)) is applied to the binary image B_3 (line 4). Next, if there is a row j in R_3 such as $g(j)$ is equal do zero, then, the bottom limit of R_3 is found and the algorithm ends (lines 5–10). Otherwise, the
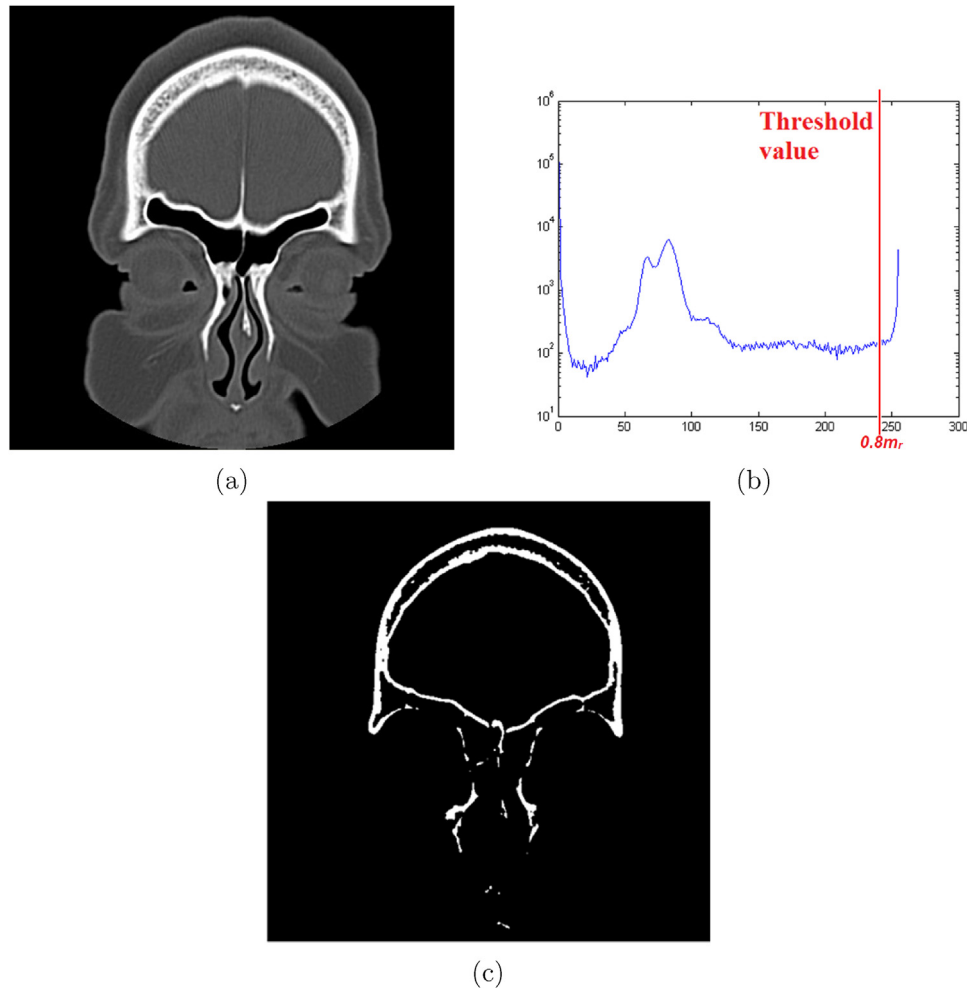
Fig. 3. (a) Gray level CT image; (b) logarithm of the gray level histogram of the CT image presented in (a) with the threshold value ($0.8m_r$) represented by the vertical red straight line; (c) binary image B_1 obtained with the binarization process, using the threshold value found automatically from the gray level histogram. (For interpretation of the references to color in this figure legend, the reader is referred to the web version of this article.)

central row of B_3, called h_{R_2}, is calculated (line 11) and the white connected regions of B_3 are stored into a list S (line 13). Next, while a white region S_i exists in S, its centroid is calculated (line 16). If such centroid is above h_{R_2} and the S_i structure is completely above h_{R_2}, this region is added to the new image Img being created with the white connected regions that compose the frontal sinus (lines 15–22). Finally, the final top and bottom limits of R_3 are taken as the top and the bottom limits of Img. The left and the right limits of R_3 are taken as the left and the right limits of R_2.

Fig. 8 shows an example of ROI R_2 defined in the first part of Algorithm 1 (line 3–10). Fig. 9 shows an example of ROI R_2 that contains regions that do not belong to the frontal sinus. In this case, the second part of Algorithm 1 (lines 11–24) is executed. In the example presented in Fig. 9, one can observe that the horizontal straight line divides R_2 in two parts. In this figure, the regions are colored with different colors. The blue regions belong to the frontal sinus. The other regions (yellow, red, orange and green) represent other cranial structures. Because the centroids of red region are below h_{R_2}, they are removed. Green regions are too small, then they are removed as well. Yellow regions are located in the border of the ROI, so they are removed too. Although the centroid of orange region is above h_{R_2}, it is not completely above h_{R_2}, then this region is discarded. All these steps are necessary because it is difficult to find the bottom limit of the ROI R_3 due to the great variances of the bone structures in this region of the cranium.

Fig. 10 illustrates the automatic frontal sinus ROI detection method in CT images proposed in our work. Initially, the ROIs R_1 (yellow rectangle) and R_2 (green rectangle) are calculated in order to guide the final ROI detection, R_3 (red rectangle).

After finding the ROI R_3, the goal is to segment both left and right frontal sinus hemispheres, which is carried out by using the centroids of each connected components inside R_3. These centroids are used to classify each component as belonging to the left or to the right side of ROI R_3. Fig. 11(a) and (b) show the binary images containing the left and right hemispheres of the frontal sinus, respectively, obtained from the ROI R_3.

Fig. 12 presents a diagram that summarizes all steps of the proposed method for automatic segmentation of the left and right hemispheres of the frontal sinuses from CT images.

3.2. Frontal sinus feature extraction

The frontal sinus descriptor adopted in our work is the Beam Angle Statistics (BAS) shape descriptor, proposed by Arica and Vural [18], extracted from the left and right frontal sinus hemispheres. BAS descriptor was chosen because it presents very good results in a number of shape analysis and recognition problems [19,20].

The Beam Angle Statistics (BAS) method is a consistent two-dimensional (2D) shape descriptor based on the 2D shape
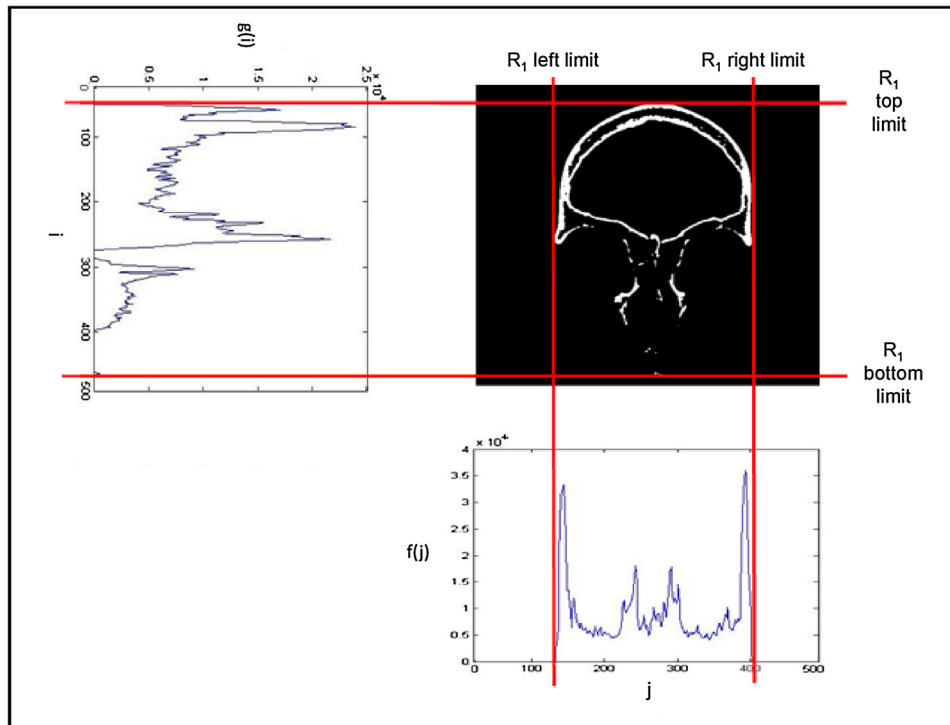
Fig. 4. Illustration of the method proposed to find the ROI R_1.

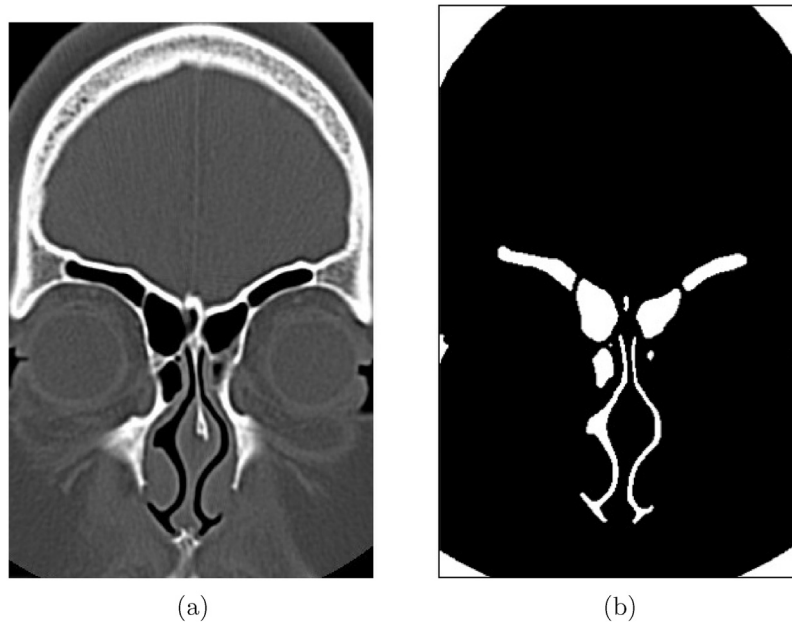(a)   (b)

Fig. 5. (a) Image I_2 obtained by cropping the image I using R_1 limits; (b) binary image B_2, the binarization of I_2.

representation. In this method an object's boundary OB is represented as a connected sequence of points $p_i = (x_i, y_i)$, $i = 1, 2, \ldots, n$, where n is the number of points that belongs to the object's boundary, and $p_i = p_{i+n}$, i.e., the sequence of points is circular.

Adopting a boundary point p_i and considering the angle $c_j(i)$ between the two vector originating at p_{i-j} and p_{i+j}, with j varying from 1 to $n/2$, as a random variable (C_i), it can be associated with p_i the first, second and third moments of this variable (mean, variance and skewness, respectively). This process is repeated for all points belonging to the OB boundary, resulting in the first, second and third moment-based functions (1D functions). Then, the feature vector is built by sampling the 1D function at k equally spaced positions of the boundary.

Since the segmented frontal sinus hemispheres in the first stage may be not connected, as one can observe in Fig. 11, a morphological closing operation is applied. After this closing operation, BAS descriptors are extracted from the fully connected left and right frontal sinus hemispheres. The feature vector of a CT scan is finally defined as the concatenation of all BAS descriptors
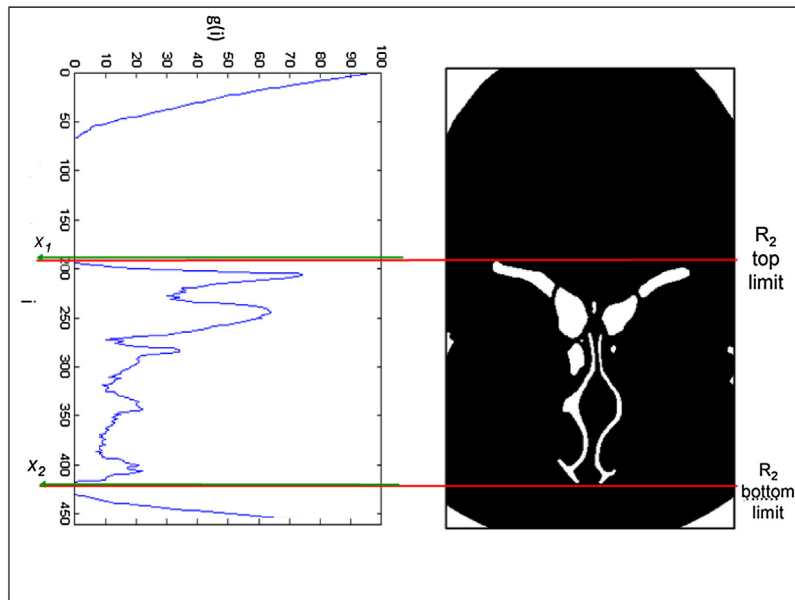
Fig. 6. Illustration of the proposed method to find the ROI R_2.

extracted from the left and the right hemispheres of all images that compose the CT scan.

3.3. Frontal sinus recognition

In the recognition stage of our method, the frontal sinus feature vectors of the probe (Π) and gallery (Γ) CT images are compared, using the L_2 distance (Euclidian distance), according to Eq. (4).

$$D(\Pi, \Gamma) = \sqrt{\sum_{i=1}^{k} (\Pi(i) - \Gamma(i))^2} \qquad (4)$$

where k is the feature vector size.

Given a query frontal sinus CT sequence of images, its classification is performed by comparing the similarity of its feature vector, Π, with each gallery feature vector, Γ, associated to each individual in the database. The assigned identity will be the one associated with the gallery identity whose feature vector Γ has minimum L_2 distance to the query feature vector Π. Fig. 13 illustrates the recognition stage of our method.

4. Assessment protocol

This section presents the ground truth and the agreement measure between the ground truth and the automatic segmentation obtained by our algorithm. It also presents the approach adopted in our experiments for obtaining the genuine and impostor matching score distributions, as well as the ROC

Fig. 7. Binary image B_3.

Fig. 8. Example of ROI R_2 for what the application of the first part of Algorithm 1 (lines 3–10) is enough to find the bottom limit (red line) of the ROI R_3 containing only the frontal sinus regions. (For interpretation of the references to color in this figure legend, the reader is referred to the web version of this article.)
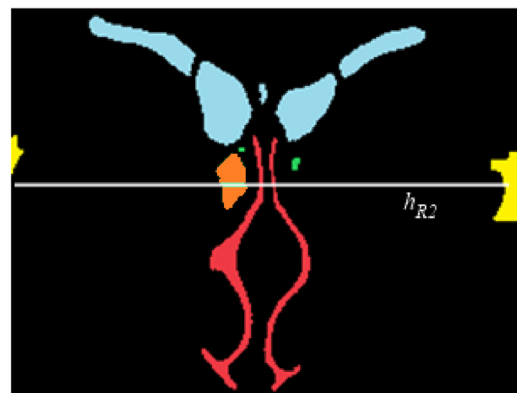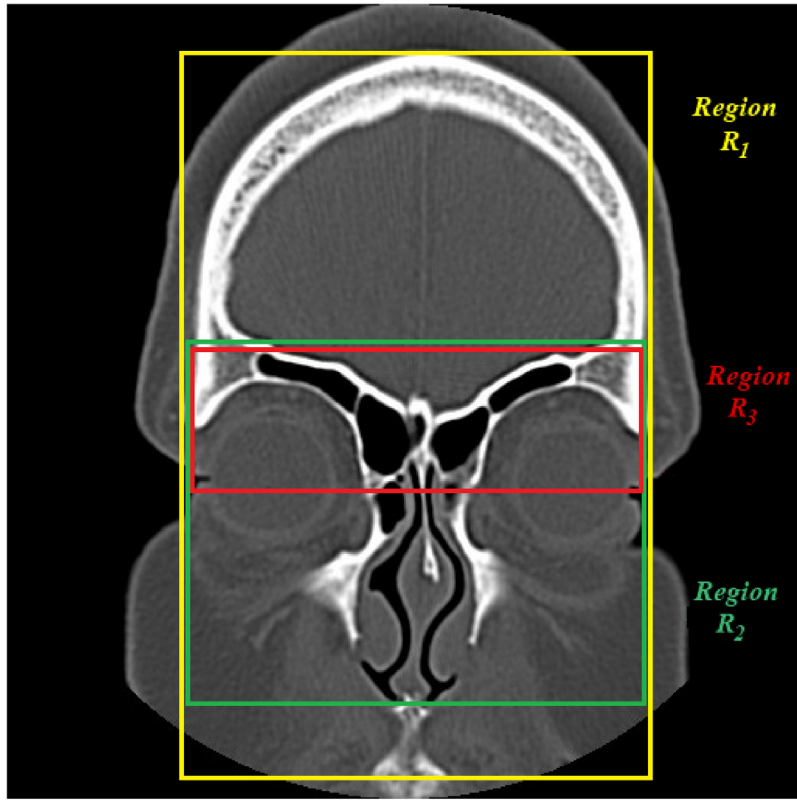

Fig. 9. Example of ROI R_2 for what the application of the second part of Algorithm 1 (lines 11–24) is necessary to find the correct bottom limit of the ROI R_3, keeping only the frontal sinus regions. (For interpretation of the references to color in this figure legend, the reader is referred to the web version of this article.)

Fig. 10. Illustration of the automatic frontal sinus ROI detection method in CT images proposed in our work. Initial ROIs: R_1 (yellow) and R_2 (green). Final ROI, R_3 (red), containing the frontal sinus.

Fig. 11. (a) Right hemisphere of the frontal sinus detected inside the ROI R_3; (b) left hemisphere of the frontal sinus detected inside the ROI R_3.
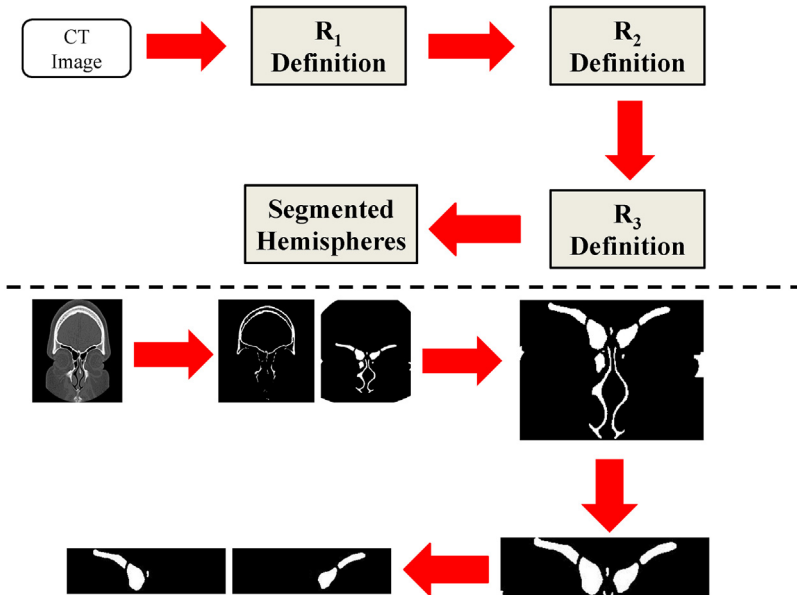
Fig. 12. Diagram of the proposed method for automatic CT frontal sinus image segmentation.
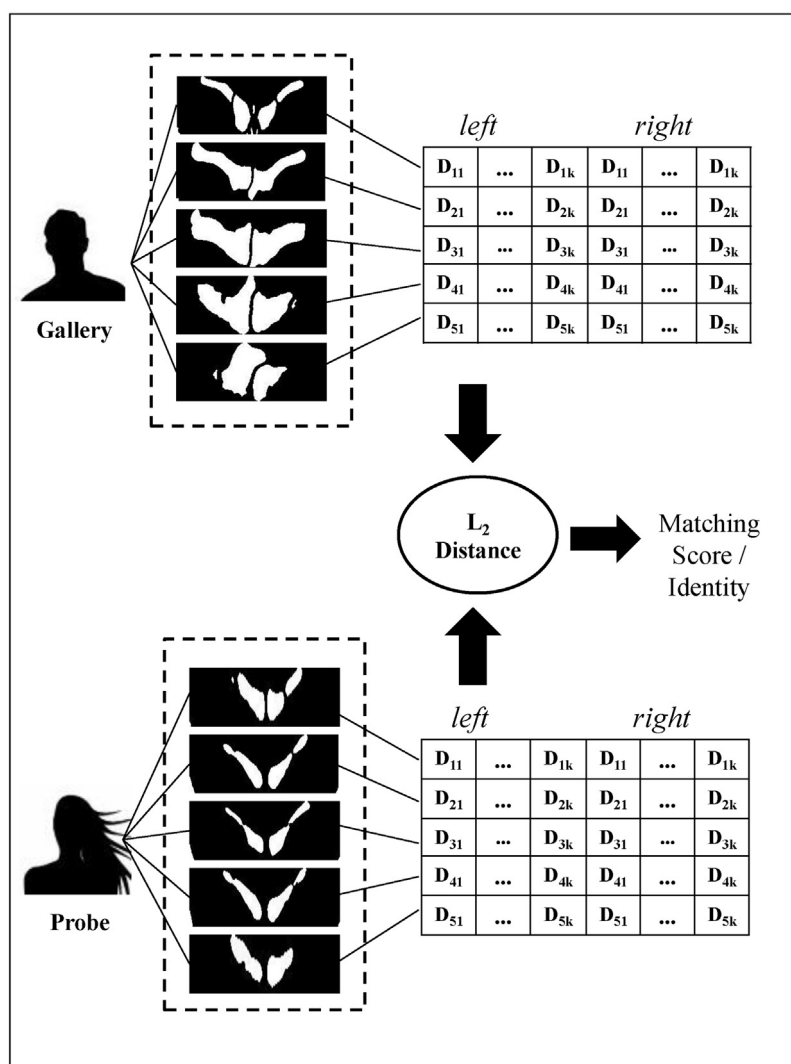
Fig. 13. Frontal sinus recognition using BAS shape descriptor method extracted from the probe and gallery CT images. The frontal sinus descriptors result from the concatenation of the BAS descriptors extracted from the left and right hemispheres of the five gallery and probe images obtained in the CT scan. The gallery and probe descriptors are compared by using the L_2 distance.

(Receiver Operating Characteristic) and CMC (Cumulative Match Characteristic) curves, used to assess the performance of our frontal sinus automatic recognition method.

4.1. Ground truth

In order to evaluate the performance of the automatic frontal sinus segmentation method proposed in this work, it was necessary to use a ground truth dataset. Therefore, we carried out the manual segmentation of all frontal sinus images of our database. To perform such manual segmentation, the ImageJ[1] software was used. With this software, upon a new layer over the image, the frontal sinus border was manually lined out by using the mouse device. The manual segmentation was evaluated and validated by a Professor, expert in Radiology and Head and Neck Surgery, of the Botucatu Medical School, UNESP, campus of Botucatu, São Paulo, Brazil.

4.2. Agreement measure of manual and automatic frontal sinus segmentation

In order to evaluate the results obtained by our automatic frontal sinus segmentation method, the Cohens Kappa coefficient was used as a measure of agreement with the manual segmentation (our ground truth dataset).

The Cohens Kappa coefficient is given by [21]:

$$KAP = \frac{f_a - f_c}{N - f_c} \tag{5}$$

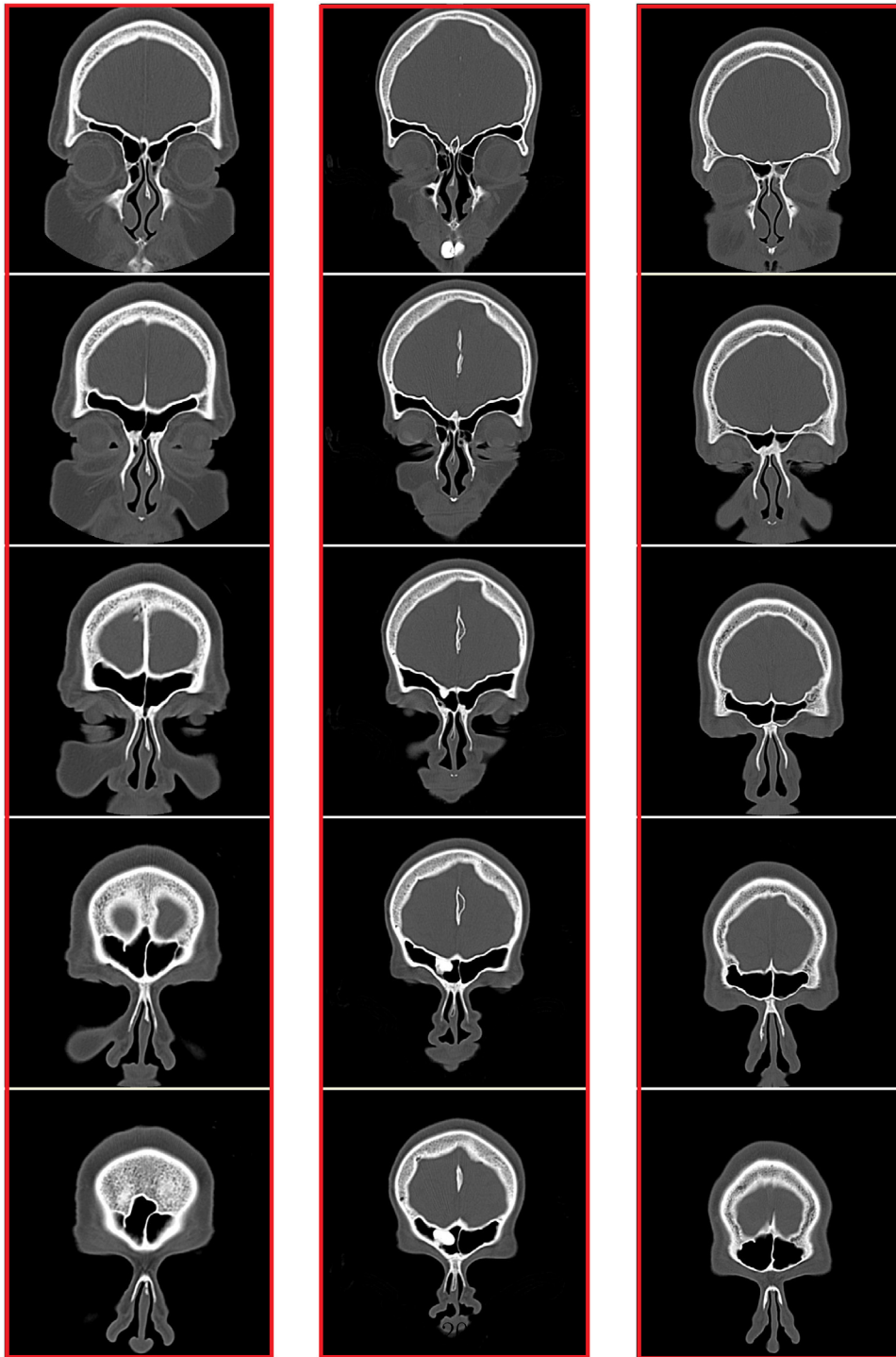where N is the total number of observations, f_a and f_c are defined as:

$$fa = TP + TN \tag{6}$$

$$fc = \frac{(TN + FN)(TN + FP) + (FP + TP)(FN + TP)}{N} \tag{7}$$

The terms in the Eqs. (6) and (7) are expressed by the overlap coordinates: True Positive (TP), True Negative (TN), False Positive

---

[1] https://imagej.nih.gov/ij/.

Fig. 14. Three sequences of CT scans of frontal sinus computed tomography (FSCT) database. Each column represents a different person.

(FP) and False Negative (FN), defined as:

$$TP = \sum_{r=1}^{|x|} \min(f_a^1(x_r), f_m^1(x_r)) \qquad (8)$$

$$FP = \sum_{r=1}^{|x|} \max(f_a^1(x_r) - f_m^1(x_r), 0) \qquad (9)$$

$$TN = \sum_{r=1}^{|x|} \min(f_a^2(x_r), f_m^2(x_r)) \qquad (10)$$

$$FN = \sum_{r=1}^{|x|} \max(f_a^2(x_r) - f_m^2(x_r), 0) \qquad (11)$$

where f_a^1 is the foreground values of the automatic segmentation result (frontal sinus), f_a^2 is the background values of the automatic segmentation result, f_m^1 is the foreground values of the manual segmentation result (frontal sinus), and f_m^2 is the background values of the manual segmentation result.

Automatic versus Manual Segmentation
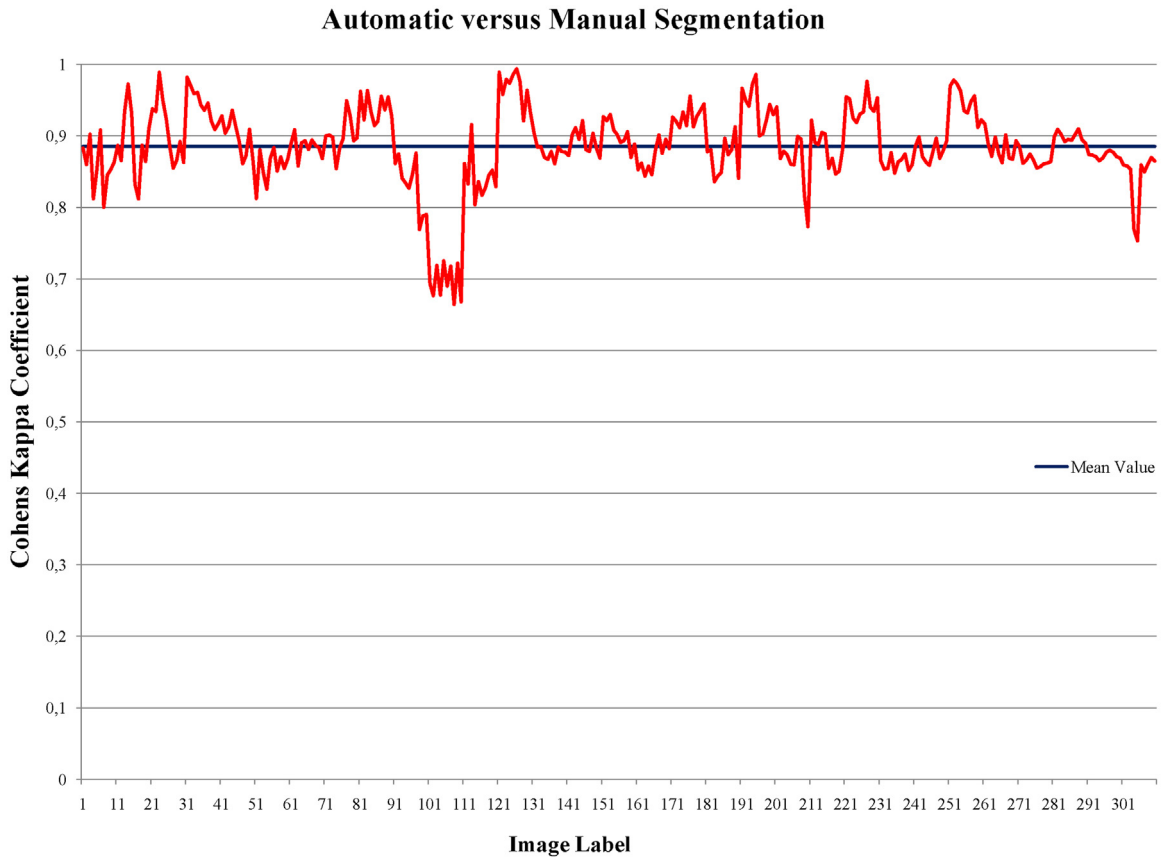
Fig. 15. Cohens Kappa coefficients between the automatic and the manual segmentations of all images from the FSCT database. The average Cohens Kappa coefficient value was 0.8852.

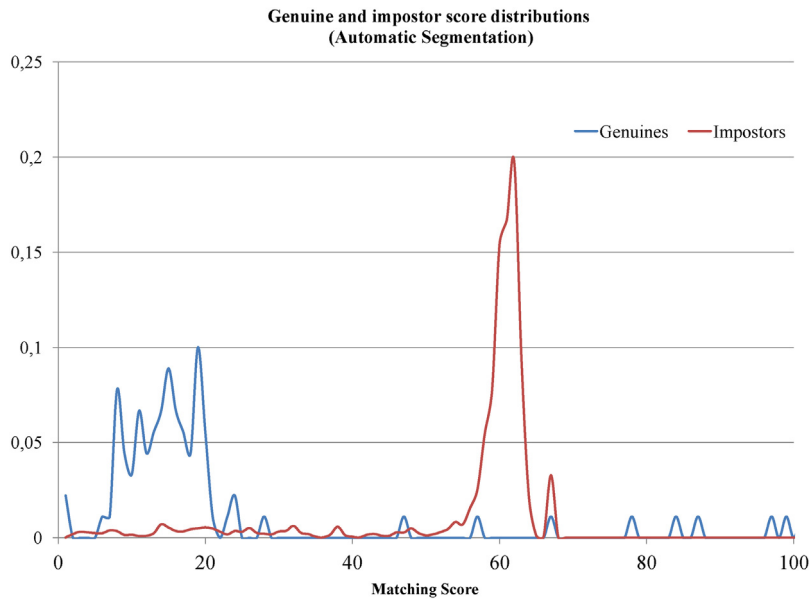### 4.3. Genuine and impostor matching score distributions

The genuine and impostor matching score distributions were calculated by comparing the frontal sinus BAS descriptors, according to the following protocol:

- **Genuine matching:** Frontal sinus descriptors extracted from different CT images of the same individual are compared and the matching scores are calculated.

- **Impostor matching:** Frontal sinus descriptors extracted from CT images of different individuals are compared and the matching scores are calculated.

4.4. Identification performance

After obtaining the genuine and the impostor matching scores, the respective genuine and impostor matching score distribution

Fig. 16. Genuine and impostor score distributions obtained by the proposed method using BAS shape descriptors.
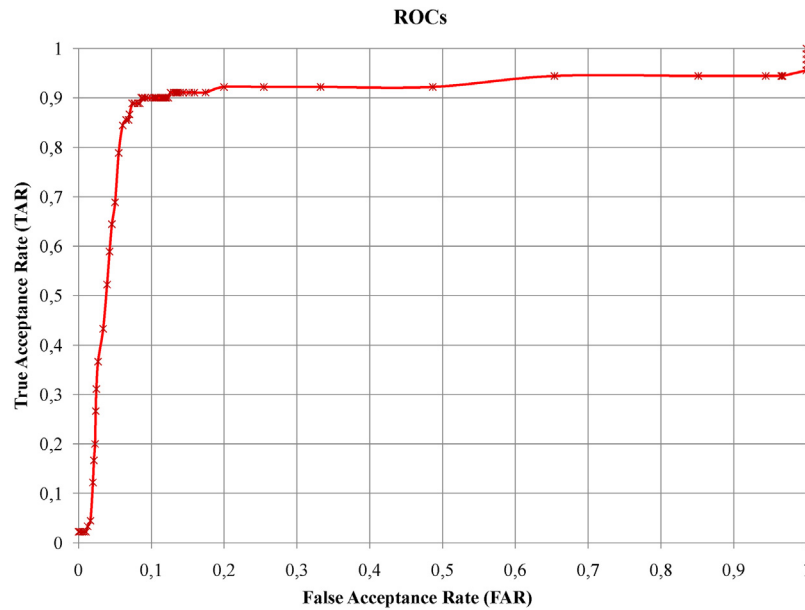
ROCs

Fig. 17. ROC curve obtained by the proposed method using BAS shape descriptors.
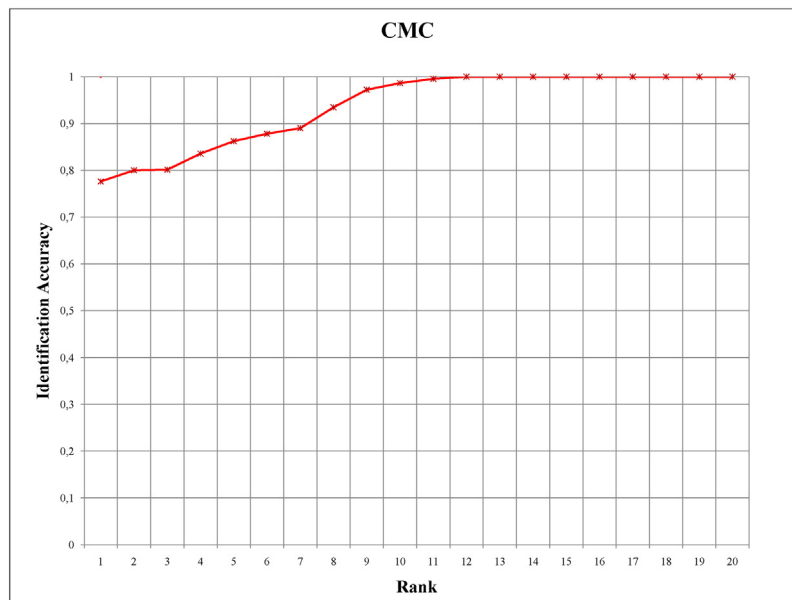
CMC

Fig. 18. CMC curve obtained by the proposed method using BAS shape descriptors.

curves are calculated, as well as the Equal Error Rate (EER), the ROC curve and the CMC curve.

The EER refers to the score value (threshold) for which the false rejection rate (FRR) is equal to the false acceptance rate (FAR).

The performance of a verification system is summarized using ROC curve, which is the plot of the false acceptance rate (FAR) against the true acceptance rate (TAR = 1 − FRR).

The performance of a closed-set identification system is summarized using CMC curve, which presents the accuracy in the identification mode for different rank values. In order to

calculate the CMC curve, each probe biometric sample is compared against all gallery samples. Then, the resulting matching scores are sorted and ranked. The CMC curve determines the rank at which a true match occurs.

5. Experimental results

This section presents the frontal sinus computed tomography (FSCT) database used in this work and the experimental results obtained with the new automatic frontal sinus recognition method.

5.1. Frontal sinus computed tomography database

The frontal sinus computed tomography (FSCT) database used in this work is composed of 310 images, obtained from two CT scans of 31 individuals older than 20-years-old from the archives of the Hospital Estadual de Bauru, Bauru, São Paulo, Brazil. Each CT scan is composed by a sequence of five images. Fig. 14 shows three sequences (columns) of five images obtained from CT scans of three distinct individuals of our FSCT database.

5.2. Frontal sinus segmentation

As already mentioned, the performance of the automatic frontal sinus segmentation method proposed in this work was assessed by means of the Cohens Kappa coefficient computed between the automatic and the manual (ground truth) segmentation of all images of our FSCT database. Fig. 15 shows the coefficients obtained for all the images of our database. The average Kappa coefficient for all images was $\overline{x_i} = 0.8852$, with a standard deviation $\sigma = 0.05$. This good result shows the efficacy of the proposed automatic Frontal Sinus segmentation method.

5.3. Frontal sinus recognition

The assessment of the proposed frontal sinus recognition method based on CT images was carried out by analysing the EER, the ROC curve, and the CMC curve obtained in our experiments on the frontal sinus computed tomography (FSCT) database.

Fig. 16 shows the genuine and impostor score matching distributions obtained using the BAS shape descriptors and the protocol defined in Section 4.3.

Fig. 17 shows the ROC curve. The EER value was equal to 8.89%, which can be considered a good result.

Fig. 18 shows the CMC curve. At rank 1, the identification accuracy was 77.25%, at rank 5, the identification accuracy was 86.91%. The identification accuracy of 100% was reached at rank 12. These results also can be considered good for this application.

6. Conclusion

The new method proposed in this work for automatic frontal sinus recognition based on computed tomography images obtained results that corroborate the results of other works in literature that affirm that frontal sinus can be successfully used for person identification.

Regarding the frontal sinus segmentation, the automatic segmentation proposed in our work is worth since the manual segmentation of the frontal sinus structure from radiographic images demands knowledge, hand ability, concentration, and time. The automated frontal sinus segmentation from CT images proposed in this work makes the process faster and more reliable.

The manual segmentation is a time consuming task. In our experiments, the average time needed to perform automatic segmentation of five images per CT scan was 30 s, while to perform the manual segmentation, by a person that was previously trained for this task, it was necessary more than 15 min. Besides, during the frontal sinus manual segmentation that was performed under the supervision of an expert in Radiology, it was necessary to redo some segmentations. Therefore, the exhaustive, boring and unreliable task of manual segmentation can be replaced by the automatic one.

It is important to emphasize that the fully automatic segmentation in computed tomography images, despite the high contrast of such images, is a complex image processing problem because the lack of a standard structure of the lower region of the frontal sinuses. This characteristic makes the definition of the bottom frontal sinus limit a challenging problem. However, comparing with X-ray images, the high quality of the computed tomography images makes the frontal sinus segmentation easier and more robust. In addition, the sequence of n images provided by computed tomography scans makes the matching more reliable, since in CT n genuine comparisons are executed, per scan, differently from the X-ray scan, which relies on only one image.

Regarding the frontal sinus recognition, the identification rates obtained by our new method are very promising, since at rank 1 the identification accuracy was 77.25%, and at rank 5 the accuracy was 86.91%. These values show the efficacy of the BAS (Beam Angle Statistics) shape features as frontal sinus descriptors. In future work we intend to fuse such features with geometrical features, usually adopted by the methods proposed in literature. So, this good result can be even better.

Regarding the use of CT images, because of the reduction of CT technology and storage costs, CT images have been more and more used in clinical evaluations of nasal sinus disease and head and neck surgery, resulting in an indispensable tool in the diagnosis and treatment of paranasal sinuses diseases [22]. Then, CT images will be more and more available in future.

We can conclude, therefore, that the automatic frontal sinus recognition based on characteristics extracted from computed tomography images is viable and effective, becoming an important alternative in biometric person identification systems, in which other traditional identification methods cannot be applied.

Acknowledgements

References

[1] A.K. Jain, P. Flynn, A.A. Ross, Handbook of Biometrics, Springer-Verlag New York, Inc., Secaucus, NJ, USA, 2007 ISBN 038771040X.

[2] J.-P. Tang, D.-Y. Hu, F.-H. Jiang, X.-J. Yu, Assessing forensic applications of the frontal sinus in a Chinese Han population, Forensic Sci. Int. 183 (13) (2009) 104.e1–104.e3, doi:http://dx.doi.org/10.1016/j.forsciint.2008.10.017 ISSN 0379-0738.

[3] E. Tatlisumak, G.Y. Ovali, A. Aslan, M. Asirdizer, Y. Zeyfeoglu, S. Tarhan, Identification of unknown bodies by using CT images of frontal sinus, Forensic Sci. Int. 26 (2007) 42–48.

[4] W.B. Saunders, Dorland's Illustrated Medical Dictionary, 25th ed., (2011) Philadelphia.

[5] E. Zuckerkandl, Anatomie normale et pathologique des fosses nasales: et de leurs annexes pneumatiques, vol. 1, Masson, Paris, 1895.

[6] W.L. Culbert, F.M. Law, Identification by comparison of roentgenograms: of nasal accessory sinuses and mastoid processes, J. Am. Med. Assoc. 88 (21) (1927) 1634–1636.

[7] A. Schuller, A note on the identification of skulls by X-ray pictures of the frontal sinuses, Med. J. Aust. 1 (1943) 554–557.

[8] F.d.A.Q. Ribeiro, Standardized measurements of radiographic films of the frontal sinuses: an aid to identifying unknown persons, Ear Nose Throat J. 79 (1) (2000) 26.

[9] N.J. Kirk, R.E. Wood, M. Goldstein, Skeletal identification using the frontal sinus region: a retrospective study of 39 cases, J. Forensic Sci. (2002).

[10] M.D.V.B.G. Brogdon, Forensic Radiology, CRC Press, 1998.

[11] C.B.R.B. Soares, M.S.C. Almeida, P. de Medeiros Loureiro Lopes, R.V. Beltrão, A. dos Anjos Pontual, F.M. de Moraes Ramos-Perez, J.N. Figueroa, M.L. dos Anjos Pontual, Human identification study by means of frontal sinus imaginological aspects, Forensic Sci. Int. 262 (2016) 183–189, doi:http://dx.doi.org/10.1016/j.forsciint.2016.03.030 ISSN 0379-0738.

[12] N. Hashim, N. Hemalatha, K. Thangaraj, A. Kareem, A. Ahmed, N.F.N. Hassan, P.T.A. Jayaprakash, Practical relevance of prescribing superimposition for determining a frontal sinus pattern match, Forensic Sci. Int. 253 (2015) 137e1–137e7.

[13] K.A. Rabelo, M.L.A. Pontual, N.Q.J. ao, K.M. Paiva, F.M.M. Ramos-Perez, M.S. Santos, A.A. Pontual, Human identification by FSS system adapted to cephalometric radiographs, Forensic Sci. Int. 262 (2016) 232–277.

[14] C. Belaldavar, V.S. Kotrashetti, S.R. Hallikerimath, A.D. Kale, Assessment of frontal sinus dimensions to determine sexual dimorphism among Indian adults, J. Forensic Dent. Sci. 6 (1) (2014) 25–30.

[15] A.T. Uthman, N.H. Al-Hawi, A.S. Al-Naaimi, A.S. Tawfeeq, E.H. Suhail, Evaluation of frontal sinus and skull measurements using spiral CT scanning: an aid in unknown person identification, J. Forensic Sci. 56 (2) (2009) 403–408.

[16] S.P.M. Carvalho, R.H.A. Silva, C. Lopes-Júnior, A.S. Peres, A utilização de imagens na identificação humana em Odontologia Legal, Radiol. Bras. 42 (2) (2009) 125–130.

[17] T.A. Xavier, A.S.S.D. Terada, R.H.A. Silva, Forensic application of the frontal and maxillary sinuses: a literature review, J. Forensic Radiol. Imaging 3 (2015) 105–110.

[18] N. Arica, F.T.Y. Vural, BAS: a perceptual shape descriptor based on the beam angle statistics, Pattern Recognit. Lett. 24 (2003) 1627–1639.

[19] G.B. Souza, A.N. Marana, Frontal Sinus Recognition: A Comparison Among Different Shape Descriptors, WVC – Workshop de Vis ao Computacional, (2013) .

[20] G.B.D. Souza, A.N. Marana, HTS and HTSn: new shape descriptors based on Hough transform statistics, Comput. Vis. Image Underst. 127 (2014) 43–56, doi:http://dx.doi.org/10.1016/j.cviu.2014.06.010 ISSN 1077-3142.

[21] J. Cohen, A coefficient of agreement for nominal scales, Educ. Psychol. Meas. 20 (1960) 37–46.

[22] A.A. Taha, A. Hanbury, Metrics for evaluating 3D medical image segmentation: analysis, selection and tool, BMC Medical Imaging (2015) 15–29.